https://doi.org/10.5194/essd-2026-401
Preprint. Discussion started: 24 June 2026

Open Access Earth System Science Data Discussions

COMBUST: Gridded combustible mass estimates of the built environment in the conterminous United States (1975-2020)

Johannes H. Uhl[1,2,3], Maxwell C. Cook[2,4], Cibele Amaral[2,5], Stefan Leyk[1,4], Jennifer K. Balch[2,4,5], Alan Robock[6], Owen B. Toon[7]

[1]University of Colorado Boulder, Institute of Behavioral Science, 483 UCB, Boulder, CO-80309, USA.
[2]University of Colorado Boulder, Earth Lab, Cooperative Institute for Research in Environmental Sciences (CIRES), 216 UCB, Boulder, CO-80309, USA.
[3]European Commission, Joint Research Centre (JRC), Via E. Fermi 2749, 21027 Ispra, Italy
[4]University of Colorado Boulder, Department of Geography, 260 UCB, Boulder, CO-80309, USA.
[5]University of Colorado Boulder, Environmental Data Science Innovation & Inclusion Lab (ESIIL), 216 UCB, Boulder, CO-80309, USA.
[6]Department of Environmental Sciences, Rutgers University, 14 College Farm Rd, New Brunswick, NJ-08901, USA.
[7]Department of Atmospheric and Oceanic Sciences, Laboratory for Atmospheric and Space Physics, University of Colorado Boulder, 311 UCB, Boulder, CO-80309, USA.

Correspondence to: Stefan Leyk (stefan.leyk@colorado.edu)

Abstract. The increasing occurrence of natural hazards such as wildfires and drought, along with urban expansion and land consumption, causes increasing levels of fire risk to populations and human settlements. Moreover, increasing geopolitical instability in many regions of the world requires evaluation of scenarios related to potential hazards caused by military operations. Quantitative knowledge of burnable fuels and their spatiotemporal distribution across landscapes is crucial for risk and potential damage assessments. While there is a good understanding of the distributions of biomass fuels based on remote sensing observations, the combustible mass of the built environment has rarely been quantified in a spatially explicit and detailed manner. Therefore, we developed fine-grained estimates of urban fuels for the conterminous United States, estimating the combustible mass of building materials, building contents, and personal vehicles at 250 m spatial resolution. The resulting dataset is called COMBUST (COmbustible Mass of the Built environment in the conterminous United STates) and is currently the most comprehensive dataset of combustible mass and materials for the U.S., covering over 110 million structures. COMBUST includes different backcasting scenarios from 1975 to 2020 and is based on the integration of a variety of geospatial data sources such as Earth-observation derived data, real estate data, statistical estimates and volunteered geographic information. COMBUST is accompanied by COMBUST Plus, a set of consistently enumerated gridded datasets facilitating combustion exposure modelling of buildings and population. These datasets constitute a rich resource for ecological and social science applications, as well as for disaster risk management, planning and decision making. COMBUST is available at https://doi.org/10.5281/zenodo.15611963.

https://doi.org/10.5194/essd-2026-401
Preprint. Discussion started: 24 June 2026

1 Introduction

Natural and human-made disasters, such as wildfires and war, can have major consequences for our built environment, yet there is relatively scarce fine-scaled information on what is at risk. The increasing occurrence of hazards such as wildfires and drought, alongside expanding rural and urban development and land conversion, causes increasing levels of fire risk to populations and human settlements, particularly where they intermingle with flammable vegetation, a transition zone known as the wildland-urban interface (WUI) (Steward et al., 2007, Radeloff et al., 2018, Mietkiewicz et al., 2020, Cheng et al., 2024). Moreover, increasing geopolitical instability in many regions of the world requires reconsideration and risk evaluation of different scenarios of military operations and their potential impact on society. These developments catalyze the need for improved assessments of the exposure of people and infrastructure and thus quantitative, fine-grained information on the human habitat, herein the built environment. While there is a good understanding of human settlements in urban areas, in particular in data-rich countries, our quantitative knowledge of where people live and how people build is surprisingly sparse. These limitations impede the consistent measurement of long-term changes in the built environment over extended time periods and across large spatial extents. Specifically, building-level information relevant to natural hazards or potential outcomes of political conflict, such as building material, building volume, and the mass of built-up structures, is scarce. Such data are crucial for risk and damage assessment, given the rapid growth of planned or unplanned, urban and rural settlements, increasingly dense and heterogeneous urban spaces, and the urgent need for building resilient and sustainable infrastructure.

Of particular interest are estimates of volume and material of built-up structures, which can be used to determine their fuel mass, or combustible mass (Frishcosy et al., 2021). While biomass fuel in natural ecosystems has been widely studied and quantified, using remotely sensed Earth observation data (e.g., Burgan et al., 1998, Reeves et al., 2009, Dubayah et al., 2020, Leite et al., 2022), the fuel of built-up structures is rarely quantified, often due to a lack of suitable data. Yet, in just the last five years, the U.S. has seen more than $81 billion in losses and more than 60,000 structures destroyed by wildfires (St. Denis et al., 2023). For a seamless and holistic understanding of fuel distributions along the wildland-urban interface, such data are urgently needed. For example, such fuel estimates can be used to quantify the impacts of wildfires on the built environment, to estimate emissions (Tang et al., 2025) and their impact on air quality (National Academy of Sciences, 2022), to model fire spread between adjacent built-up structures (Mahmoud & Chulahwat, 2018), and its interactions with vegetation-based fire spread. Hence, there is a pressing need to quantify the flammability of the built environment and monitor these characteristics over time as an essential metric for integrated risk assessments and for sustainable, climate-adapted and fire-resistant development (Smith et al., 2016, McWethy et al., 2019).

Moreover, information about building mass is crucial to assess the impact of development on the environment within urban and peri-urban areas or close to unoccupied natural ecosystems. Such information could be used for studying the impacts of settlement development on hydrology, microclimate, and biodiversity within and around settlements. Building mass is also critical for the estimation of expected building debris and rubble in the case of a natural disaster such as earthquakes or

https://doi.org/10.5194/essd-2026-401
Preprint. Discussion started: 24 June 2026

landslides (Ural et al., 2011, Du et al., 2013) to facilitate and support effective disaster response and risk management. Combined aspects of flammability, resilience and mass are also crucial in efforts to estimate the potential impact in scenarios of war, armed conflict and missile strikes. In such scenarios, it is crucial to understand possible damages, the material that might burn and the amount or mass of the built environment.

For example, studies of the environmental impacts of nuclear wars show that smoke and soot from burning cities can reach the stratosphere in sufficient quantities to produce devastating climate changes, threatening the bulk of humanity with agricultural disaster and starvation (Turco et al., 1983, 1990, Robock et al., 2007a,b, Stenke et al., 2013, Pausata et al., 2016, Coupe et al. 2019, Toon et al., 2019, Xia et al., 2022). These studies require estimates of fuel loads from urban materials at extensive spatial coverage. Since the emission factors vary with the type of material burning, the fuel load needs to differentiate a variety of materials, including wood and lumber, paper, plastics and polymers, hydrocarbons, asphalt, and cloth. Previous studies, such as Turco et al. (1990), primarily estimated fuel loads using top-down approaches to calculate the total amount of material in use. Toon et al. (2007, 2008) summarized this approach by assigning 11 metric tons of fuel to each person in the developed world. The types of fuels were assumed to be constant and based on top-down surveys of fuel types. Fuel loads for a small number of cities were measured, indicating that fuel loads were proportional to population density (Toon et al., 2007). However, building materials vary from place to place, the types of fuel in buildings have changed over time, in particular as the use of plastics has increased, and the amount of fuel per person may vary greatly with population density, wealth, and cultural trends. Therefore, detailed data of fuel loads at fine spatial and temporal resolutions are needed to estimate the impacts of war-related disasters, in a more sophisticated manner at regional and local scales.

While fine-grained data on built-up areas can be obtained from Earth observation data (e.g., Pesaresi et al., 2024, Marconcini et al., 2020a), covering relatively long temporal windows (i.e., since the 1970s or 1980s; Gong et al., 2020, Marconcini et al., 2020b, Pesaresi et al., 2024), only recently, large-scale mapping efforts on the vertical component of the built environment have been initiated (Pesaresi et al, 2021, Esch et al., 2022, Che et al., 2024, Ma et al., 2024, Florio et al., 2025, Oostwegel et al., 2025, Zhu et al., 2026). While such data enable the geometric description of the built environment at a fine grain, data on other properties, such as building material or function, are rare and do not capture temporal dynamics (Haberl et al., 2021, Frantz et al., 2023, Haberl et al., 2025). However, longitudinal urban data are key to fully understand urban dynamics (Papini et al., 2025), and knowledge of these properties and their changes over time is crucial for the quantification and evolution of mass and flammable material contained in buildings. Hence, alternative data sources need to be exploited, such as real estate, cadastral or tax assessment data, often containing field survey or manually verified data. Such data are increasingly made available to the public, by governmental authorities (Uhl & Leyk, 2022) or via industry-fueled data production efforts (Leyk et al., 2020) and offer unique opportunities for scientific studies of the built environment (Nolte et al., 2023).

Herein, we make use of different data sources to quantify and evaluate the combustible mass of the built environment in the conterminous United States (CONUS) over time. Specifically, we integrate the “Material stock map of CONUS” dataset (MSMC; Frantz et al. 2023), the Zillow Transaction and Assessment Dataset (ZTRAX; Zillow 2020), Microsoft’s

https://doi.org/10.5194/essd-2026-401
Preprint. Discussion started: 24 June 2026

USBuildingFootprints dataset (Microsoft 2021), historical building volume and population data from the Global Human Settlement Layer (GHSL; Pesaresi et al., 2024), as well as historical building densities from the HISDAC-US dataset (Leyk & Uhl, 2018), among other data sources, enumerated in gridded spatial layers of 250 m × 250 m, semidecadally from 1975 to 2020, and call this dataset COMBUST (COmbustible Mass of the Built environment in the conterminous United STates). This data harmonization effort integrates across over 110 million individual structures (1975-2020) and is currently the most comprehensive dataset of combustible mass and material for the United States. COMBUST is publicly available (Uhl et al., 2025) and is accompanied by COMBUST Plus, a set of gridded surfaces for population and building exposure analysis to be used in conjunction with COMBUST. Herein, we describe the COMBUST dataset (Section 2), the source data and methods to produce COMBUST (Section 3), and showcase the data and high-level findings (Section 4). Section 5 concludes with a discussion of the limitations of COMBUST.

2 Dataset description

COMBUST consists of a large set of almost 200 gridded datasets in GeoTIFF format, referenced in Albers Equal Area Conic projection for the conterminous US (EPSG:5070), enumerated in grid cells of 250m x 250m, aligned to the grid of the Historical Settlement Data Compilation for the U.S. (HISDAC-US, Leyk and Uhl, 2018). All mass estimates are reported as total tons per grid cell. The suffixes "low", "mean", and "high" denote the three scenarios implemented in the MSMC data (Frantz et al. 2023). COMBUST is organized in 9 ZIP archives, one for each of the nine themes (see below).

2.1 Themes and components of the COMBUST dataset

1. Combustible mass by component: building contents, building material, personal vehicles, gas stations, refineries. (2020)
2. COMBUST-Plus: Thematic layers of the built environment and biomass for exposure and interaction modelling (2010-2020)
3. Combustible mass of buildings and their content by material (2020)
4. Combustible mass of buildings and their content by material type (2020)
5. Historical estimates of combustible mass of personal vehicles (1975-2020), by material (1995-2020)
6. Historical estimates of combustible mass of buildings - 1975-2020 (5-yr intervals), model 1 (using HISDAC-US building indoor area change rates)
7. Historical estimates of combustible mass of buildings - 1975-2020 (5-yr intervals), model 2 (using HISDAC-US historical building density change rates)
8. Historical estimates of combustible mass of buildings - 1975-2020 (5-yr intervals), model 3 (using GHSL building volume change rates)
9. Mass of non-combustible materials for rubble and debris estimation (2020)

https://doi.org/10.5194/essd-2026-401
Preprint. Discussion started: 24 June 2026

Table 1 provides an overview of the themes and datasets covered in COMBUST.

Table 1. COMBUST themes and datasets

Theme	Layer description	File names
1	Total comb. mass of the built environment incl. cars	combust_cm_total_scenario_<low,mean,high>_2020.tif
	Comb. mass of building material	combust_cm_buildingmaterial_all_scenario_<low,mean,high>_2020.tif
	Comb. mass of building contents	combust_cm_buildingcontent_total_2020.tif
	Comb. mass of fuel in gas stations	combust_cm_gasstations_2020.tif
	Comb. mass of fuel in refineries	combust_cm_refineries_2020.tif
	Comb. mass of cars	combust_cm_car_total_t_2020.tif
2	Number of buildings (Source: Microsoft USBuildingFootprints)	combust_plus_num_buildings_2020.tif
	Total built-up area (Source: Microsoft USBuildingFootprints)	combust_plus_builtup_area_2020.tif
	Number of residential units (Source: HISDAC-US V2)	combust_plus_num_units_2020.tif
	Share of residential buildings (Source: HISDAC-US V2)	combust_plus_residential_building_share_2020.tif
	Average cadastral parcel size (Source: ZTRAX)	combust_plus_average_lotsize_2020.tif
	Average building construction year (Source: ZTRAX)	combust_plus_average_constr_year_2020.tif
	Earliest building construction year (Source: ZTRAX)	combust_plus_earliest_constr_year_2020.tif
	Local property ownership rate (Source: ZTRAX)	combust_plus_local_ownership_rate_2020.tif
	Resident population (Source: GHSL R2023A, GHS-POP)	combust_plus_resident_population_<1975-2020>.tif
	Above-ground combustible biomass (Source: Spawn et al. 2020)	combust_plus_combustible_biomass_aboveground_2010.tif
	Below-ground combustible biomass (Source: Spawn et al. 2020)	combust_plus_combustible_biomass_belowground_2010.tif
	Total combustible biomass (Source: Spawn et al. 2020)	combust_plus_combustible_biomass_total_2010.tif
3	Mass of combustible building contents: cloth component	combust_cm_buildingcontent_cloth.tif
	Mass of combustible building contents: paper component	combust_cm_buildingcontent_paper.tif
	Mass of combustible building contents: plastic component	combust_cm_buildingcontent_plastic.tif
	Mass of combustible building contents: wood component	combust_cm_buildingcontent_wood.tif
	Mass of combustible building materials: petrochemical-based materials	combust_cm_buildingmaterial_all_other_petrochemical_based_materials_scenario_<low,mean,high>.tif
	Mass of combustible building materials: bitumen	combust_cm_buildingmaterial_bitumen_scenario_<low,mean,high>.tif
	Mass of combustible building materials: other biomass-based materials	combust_cm_buildingmaterial_other_biomass_based_materials_scenario_<low,mean,high>.tif
	Mass of combustible building materials: timber	combust_cm_buildingmaterial_timber_scenario_<low,mean,high>.tif
4	Combustible mass of buildings (commercial / industrial)	combust_cm_building_commercial_industrial_scenario_<low,mean,high>_2020.tif
	Combustible mass of buildings (commercial - inner city)	combust_cm_building_commercial_innercity_scenario_<low,mean,high>_2020.tif
	Combustible mass of buildings (highrise)	combust_cm_building_highrise_scenario_<low,mean,high>_2020.tif
	Combustible mass of buildings (lightweight)	combust_cm_building_lightweight_scenario_<low,mean,high>_2020.tif
	Combustible mass of buildings (multi-family)	combust_cm_building_multifamily_scenario_<low,mean,high>_2020.tif
	Combustible mass of buildings (single family)	combust_cm_building_singlefamily_scenario_<low,mean,high>_2020.tif

https://doi.org/10.5194/essd-2026-401
Preprint. Discussion started: 24 June 2026

	Combustible mass of buildings (skyscraper)	combust_cm_building_skyscraper_scenario_<low,mean,high>_2020.tif
5	Historical estimates of total comb. mass of personal cars of residents	combust_cm_car_total_t_<Year>.tif
	Historical estimates of comb. mass of personal cars of residents, plastic	combust_cm_car_plastic_t_<Year>.tif
	Historical estimates of comb. mass of personal cars of residents, rubber	combust_cm_car_rubber_t_<Year>.tif
	Historical estimates of comb. mass of personal cars of residents, fluids	combust_cm_car_fluidlubricants_t_<Year>.tif
6	Historical estimates of comb. mass of building since 1975, model 1, non-backcastable combustible mass	combust_cm_building_all_scenario_<low,mean,high>_backcasted_mod1_hisdacus_bui_<Year>.tif
7	Historical estimates of comb. mass of building since 1975, model 2, non-backcastable combustible mass	combust_cm_building_all_scenario_<low,mean,high>_backcasted_mod2_hisdacus_bupl_<Year>.tif
8	Historical estimates of comb. mass of building since 1975, model 3, non-backcastable combustible mass	combust_cm_building_all_scenario_<low,mean,high>_backcasted_mod3_ghsl_<Year>.tif
9	Non-combustible mass of cars, historical estimates	combust_noncombust_car_non_combmass_t_<Year>.tif
	Non-combustible mass of building materials	combust_noncombust_<low,mean,high>_noncombust_total_mass_ext_t.tif

3 Methodology

3.1 Combustible mass of buildings

Combustible mass of the building stock ($CM_{\text{Building stock}}$) is calculated as

$$CM_{\text{Building stock}} = CM_{\text{Building material}} + CM_{\text{Building content}} + CM_{\text{Gas stations}} + CM_{\text{Refineries}} \quad (1)$$

The combustible mass of **building material** has been derived from data on building volume and building mass, available for the conterminous United States at 10 m spatial resolution for the year 2018, called "Material stock map of CONUS" (Frantz et al. 2023). These data, henceforth shortened to MSMC, were aggregated to the 250 m target grid, and non-flammable materials were excluded. The mass of the following materials was taken into account: timber and other biomass-based materials, bitumen and other petrochemical-based materials used for the construction of buildings. Frantz et al. (a) used Microsoft building footprint data for the US to delineate buildings, and (b) estimated building height and building type from Sentinel-1 and Sentinel-2 Earth observation data. Based on these data, they (c) estimated building volume per 10 m grid cell and (d) used estimates of the material composition of each building type to estimate the mass of buildings (enumerated in 10 m grid cells). They finally (e) estimate a lower and an upper bound of building material mass, and report also the average of both. These three estimates are reflected in the "low", "mean", and "high" variants of the COMBUST surfaces. COMBUST reports the mass of all combustible materials, per material type, per building type, and overall. The detailed process is described in Appendix A.

https://doi.org/10.5194/essd-2026-401
Preprint. Discussion started: 24 June 2026

3.2 Combustible mass of building contents

The combustible mass of building contents has been derived using a method proposed by Frishcosy et al. (2021). While other approaches for the estimation of building content fuel loads are based on assumptions from the early 1990s (Bush et al., 1991), or focus on specific building types only (Barnett et al., 2022; Dundar & Selamet, 2023), the method proposed by Frishcosy et al. (2021) infers the mass of flammable building contents based on building indoor area and building function, allow for a spatially-explicit application of the method across different building types. Specifically, we used property-level information from the Zillow Transaction and Assessment Dataset (ZTRAX), commonly used for environmental research (Nolte et al., 2024), for the year 2020, providing building indoor area and function for a large proportion of the properties in the U.S. The research team had access to the ZTRAX dataset in the scope of a data share agreement. By applying the method from Frishcosy et al., estimates of the combustible mass of building contents were calculated, which were then aggregated to the 250 m target grid (see Appendix A for details). As the Frantz et al. building mass data are referenced to 2018, and the ZTRAX data underlying the building content mass estimates are referenced to 2020, our estimates reflect the state of the building stock between 2018 and 2020, on average 2019. For grid cells where no ZTRAX data were available (roughly 3% of CONUS counties), the combustible mass of building contents was imputed by calculating the median of cell-wise ratios $CM_{\text{Building content}}$ / $CM_{\text{Building material}}$ where both values were available, and this ratio was then used to estimate $CM_{\text{Building content}}$ based on $CM_{\text{Building material}}$ where the former was missing. This median ratio was ~13% for the "low" MSMC scenario, and ~8% for the "high" scenario. The detailed process is described in Appendix B.

3.3 Combustible mass of gas stations and refineries

The combustible mass of gas stations was estimated separately. The geolocations of almost 100,000 gas stations in the CONUS were obtained, from the OpenStreetMap database version as of September 2024. Based on an average estimate of fuel stored in gas stations, the combustible mass of fuel reserves in gas stations was estimated, and added to the grid cells in which the gas stations are located. Similarly, the combustible mass of refineries was estimated based on geolocation data from the Homeland Infrastructure Foundation-Level Database (HIFLD 2025), published in 2021, using an estimated average stock of fuels stored at refinery locations. Likewise, the estimated combustible mass was added to the grid cells in which the refineries are located.

3.4 Combustible mass of personal vehicles

We used statistics on the number of **personal vehicles** per capita, over time (Davis and Boundy 2021) and on the average weight and material composition of personal vehicles, over time. These estimates reflect changes in average car ownership, size (weight), technology (e.g., gas vs. electric cars) and material composition over time. From these material compositions, we selected combustible materials, and used gridded data on residential population distribution from the Global Human Settlement Layer (GHSL), i.e., the GHS-POP R2023A dataset to estimate the spatial distributions of combustible car

https://doi.org/10.5194/essd-2026-401
Preprint. Discussion started: 24 June 2026

material per 250 m grid cell. For that, we estimated the number of personal vehicles per grid cell (based on the average number of personal vehicles per capita and total resident population per cell). Based on the estimated number of personal vehicles per grid cell, we assigned the corresponding weight of combustible car materials to each grid cell.

3.5 Backcasting of building-related combustible mass to 1975

We implemented three models for backcasting of combustible mass from 1975 to 2020 in 5-year intervals:

- **Model 1:** Uses the historical change rates of a conflated version of HISDAC US V1 and V2 Built-up intensity (BUI) indoor area estimates (Leyk & Uhl 2018, Ahn et al. 2024) to backcast the 2020 gridded combustible mass data.
- **Model 2:** Uses the historical change rates of a conflated version of HISDAC US V1 and V2 built-up property locations (BUPL), a measure of building density, to backcast the 2020 gridded combustible mass data (Uhl et al., 2021).
- **Model 3:** Uses the historical change rates of gridded building volume estimates from the Global Human Settlement Layer (GHSL; GHS-BUILT-V R2023A) to backcast the 2020 gridded combustible mass data (Pesaresi et al., 2024).

From these datasets, the change rates with respect to the year 2020 were extracted, and applied to the 2020 combustible mass estimates. While the GHSL-based backcasting results are spatially nearly exhaustive, the HISDAC-US based backcasting results suffer from lower levels of coverage, as the historical information (derived from building construction year information from ZTRAX underlying the HISDAC-US data) is not available in some states, including parts of New Mexico, South and North Dakota, Wisconsin, and Louisiana.

3.6 Non-combustible mass estimates of buildings and cars

The materials of buildings and cars that are considered non-combustible, such as various metals, concrete and bricks were aggregated separately to estimate the total non-combustible mass of buildings and personal vehicles per 250 m grid cell, facilitating rubble and debris estimations.

3.7 COMBUST-Plus – accompanying population and building exposure variables, and combustible biomass estimates

Data on biomass carbon density, produced by Spawn et al. (2020) for the year 2010 were used to estimate the total combustible biomass per 250 m grid cell. These data were resampled from per-hectare density estimates. The combustible biomass was estimated to be 2× the reported carbon mass (Houghton et al., 2009), and this process was done separately for above-ground and below-ground biomass estimates.
Further variables in COMBUST-Plus include:

https://doi.org/10.5194/essd-2026-401
Preprint. Discussion started: 24 June 2026

1. Building density and built-up area per 250×250 m grid cell, as reported in Microsoft´s USBuildingFootprint dataset, and the average cadastral parcel size per grid cell, as reported in ZTRAX, as measures of built-up intensity.
2. Number and share of residential building units, as reported in HISDAC-US V2 (Ahn et al., 2024), to quantify the exposure of residential properties.
3. The total population per grid cell, as reported in GHSL, and the share of locally owned properties, as derived from ZTRAX. The latter allows to estimate the potential number of seasonally uninhabited residential units, for example in settlements dominated by vacation homes.
4. Average and earliest construction year per grid cell, as derived from HISDAC-US, measuring the age of the built stock that can be linked to building characteristics related to building resilience and value.

These accompanying variables allow for quantification of the exposed population, structures, and potentially for estimating building resilience and/or damage. The complete data processing workflow is shown in Fig. 1.

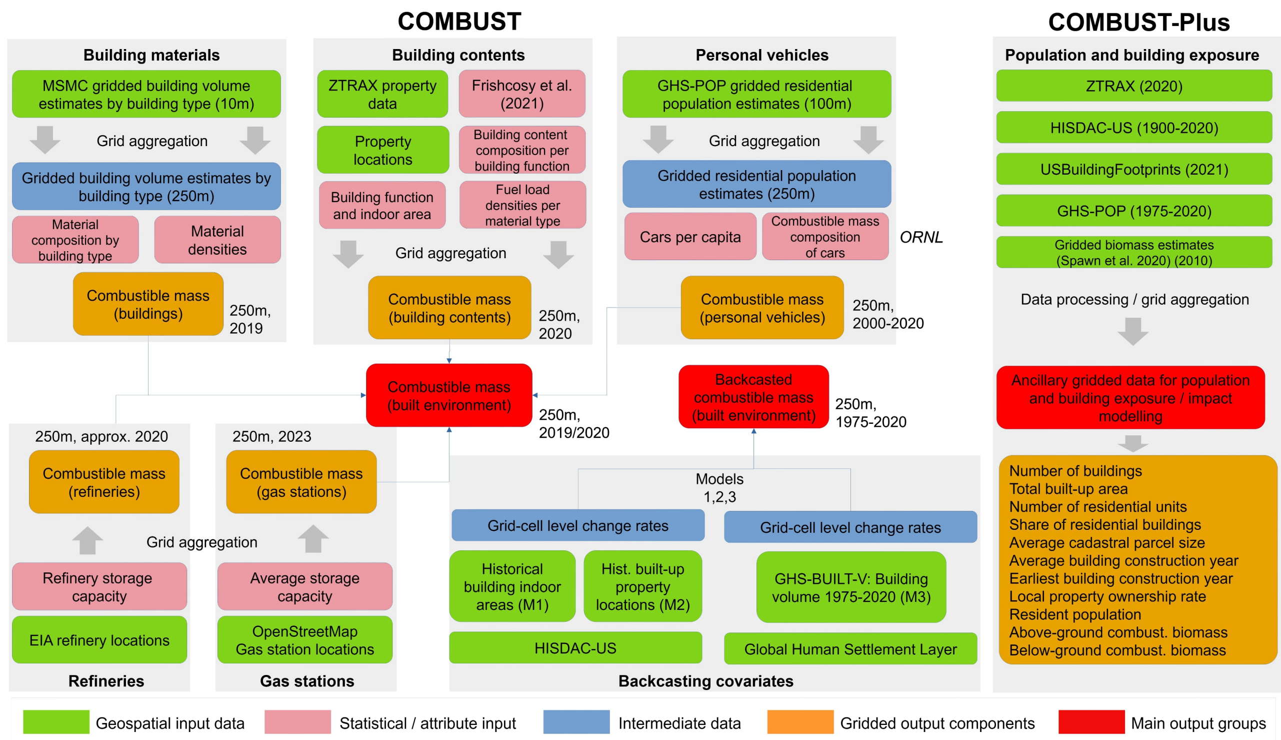

Figure 1. COMBUST data processing workflow. Explanation of acronyms: MSMC = Material stock map of CONUS; ZTRAX = Zillow Transaction and Assessment Dataset; GHS-POP: Global Human Settlement Layer population data; HISDAC-US = Historical Settlement Data Compilation for the U.S.; EIA = U.S. Energy Information Administration.

https://doi.org/10.5194/essd-2026-401
Preprint. Discussion started: 24 June 2026

4 Results

4.1 Spatial distributions of combustible mass across the conterminous U.S.

Exemplary gridded spatial layers measuring combustible mass are shown in Figures 2-4. Figure 2 shows the total combustible mass (including building materials, contents, gas stations, refineries, and personal vehicles) in selected regions of the U.S. for the year 2020, except Figure 2d showing the backcasted estimates for 1975.

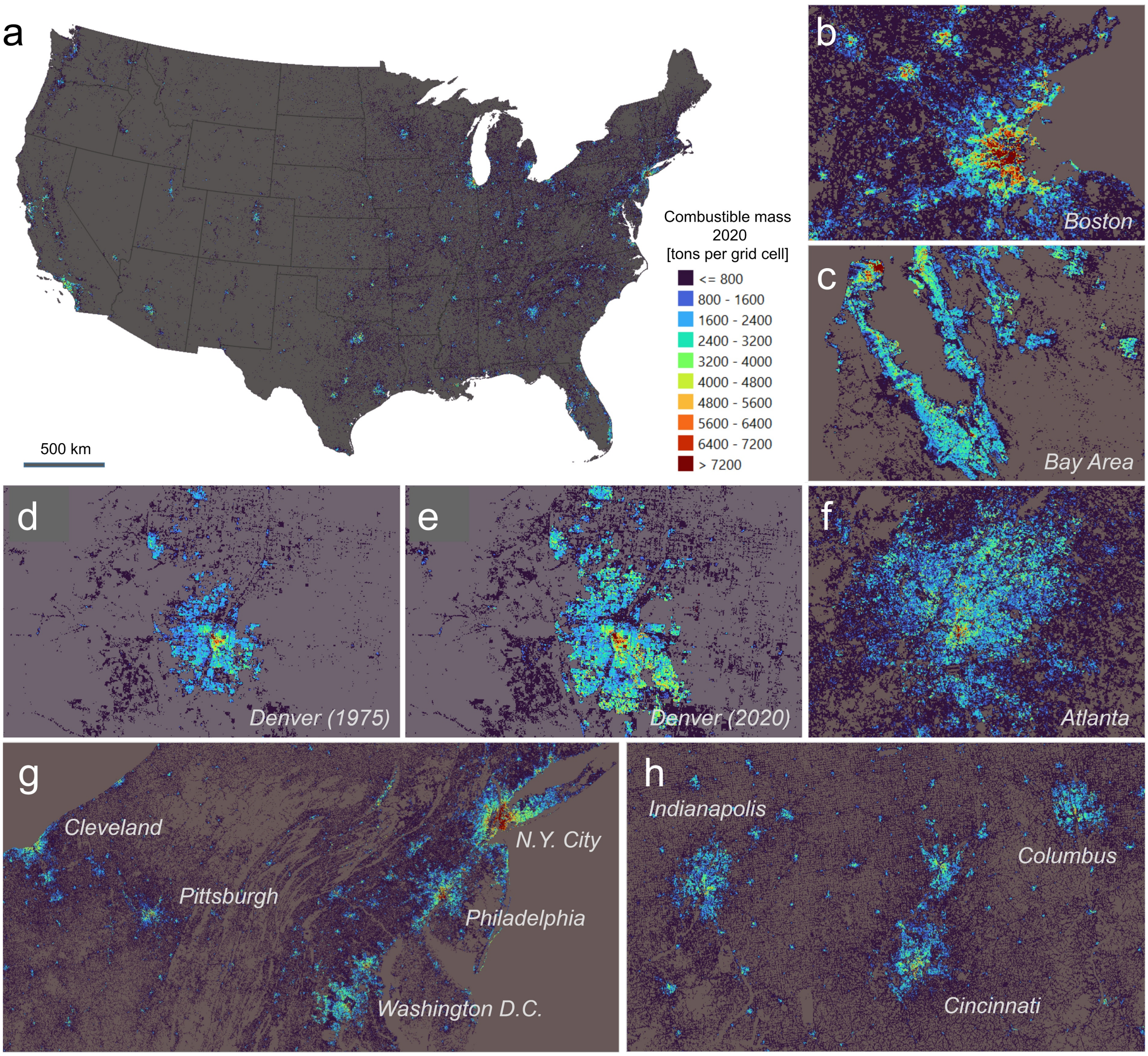

Figure 2. COMBUST 250 m gridded surface measuring combustible mass of buildings, their content, personal vehicles, gas stations and refineries (a) across the conterminous U.S. in 2020, (b) shown for the Boston and (c) Bay Area regions; combustible mass distribution in the Denver region for (d) 1975 and (e) 2020; and for 2020 in (f) Atlanta, (g) and (h) selected regions across the United States. The distribution of combustible mass in 1975 in (d) is based on Model 2 (i.e., HISDAC-US BUPL change rates) for backcasting.

https://doi.org/10.5194/essd-2026-401
Preprint. Discussion started: 24 June 2026

Open Access Earth System Science Data Discussions

Figure 3 shows the spatial distributions of the components of combustible mass, including building materials (Figure 3a,b), building contents (Figure 3c,d) and personal vehicles and gas stations (Figure 3e).

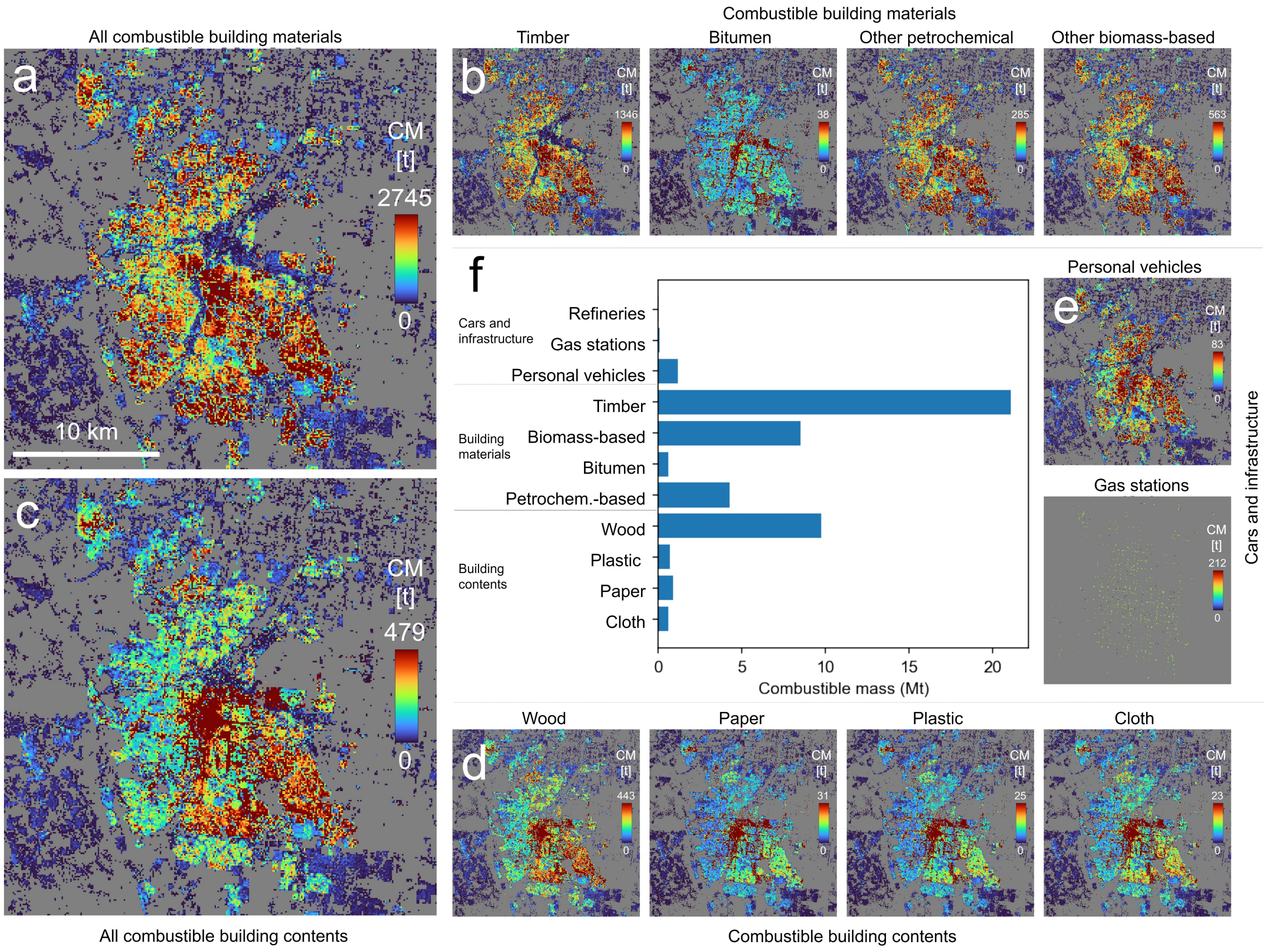

Figure 3. COMBUST 250 m gridded surfaces measuring combustible mass by component, shown for the Denver metropolitan area, Colorado, USA and the year 2020: (a) Building materials total, (b) individual building materials, (c) building contents total, (d) building contents by material, and (e) spatial distribution of combustible mass of personal vehicles and gas stations. Panel (f) shows the total material decomposition of combustible mass for the spatial extent shown in panels (a) to (e).Material types of buildings (a) are adapted from Frantz et al. 2023; building content materials (d) are adapted from Frishcosy et al. (2021).

Figure 4 shows the gridded combustible mass by building type and also the mass distribution of non-combustible materials, which represents an important spatial variable for quantifying fire spread and rubble.

https://doi.org/10.5194/essd-2026-401
Preprint. Discussion started: 24 June 2026

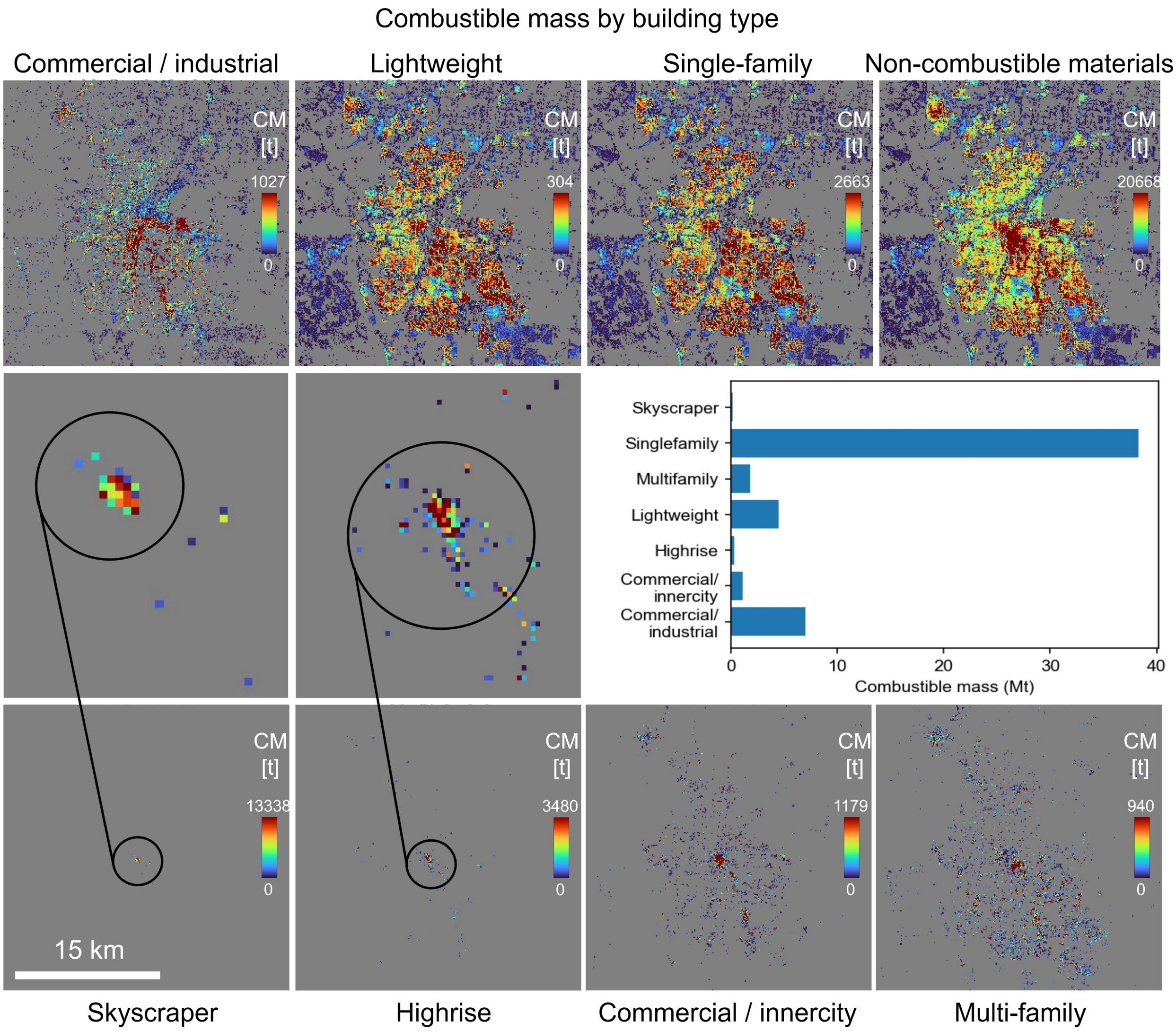

Figure 4. COMBUST 250 m gridded surfaces measuring combustible mass by building type in 2020, shown for the Denver metropolitan area, Colorado, USA. Building taxonomy adapted from Frantz et al. 2023.

4.2 Dissecting combustible mass in 2020

We estimate a total mass of 64 Gt for building materials, personal vehicles and building contents. By comparison, Frantz et al. estimate the total weight of the CONUS built environment to 127 Gt, out of which 62 Gt are the mass of building materials. Out of these 64 Gt, 55 Gt are non-combustible, and only 7.8 Gt, corresponding to 13.7%, are combustible. These 7.8 Gt represent the optimistic (upper bound) scenario from Frantz et al., while the average scenario results in a total of 6.9 Gt total combustible mass, corresponding to a total of 20.8 t of combustible mass per capita (CM/capita) in 2020. Out of

https://doi.org/10.5194/essd-2026-401
Preprint. Discussion started: 24 June 2026

these estimated 20.8 t/capita of combustible mass, around 18.2 t/capita are building material, 2.6 t/capita are estimated to be building contents, and 0.39 t/capita are combustible materials from personal vehicles (Table 2).

The large majority of the combustible mass of building materials are single-family residential homes (5.3 Gt out of 6.0 Gt in the "mean" scenario), corresponding to 16 t/capita, and the combustible mass of commercial and industrial buildings is estimated at 0.9 Gt (2.8 t/capita). Across the whole CONUS population in 2020, the combustible mass of high-rise buildings and skyscrapers only makes up around 100 kg/capita (Table 2). For comparison, the mass of combustible materials contained in personal vehicles in 2020 is estimated to be almost four times higher (i.e., 384 kg/capita; Table 2).

Table 2. Total combustible (and non-combustible) mass and mass/capita by component (see Table A.1.1 for a definition of building types).

Component	Mass (Gt)			Mass per capita (t/capita)		
	low	mean	high	low	mean	high
Total mass (building materials, contents, personal vehicles)	39.267	54.669	64.143	117.359	164.949	193.531
Total non-combustible mass (building materials)	32.687	46.490	55.014	98.617	140.262	165.981
Total combustible mass	5.289	6.911	7.846	15.957	20.850	23.671
Combustible mass of building material 2020	4.415	6.037	6.972	13.322	18.215	21.036
Combustible mass of building content 2020	0.874	0.874	0.874	2.635	2.635	2.635
Combustible mass of personal vehicles 2020	0.127	0.127	0.127	0.384	0.384	0.384
Combustible mass of gas stations 2020	0.010	0.010	0.010	0.031	0.031	0.031
Combustible mass of refineries 2020	0.001	0.001	0.001	0.003	0.003	0.003
Combustible mass of single family buildings 2020	4.167	5.304	6.041	12.572	16.002	18.227
Combustible mass of commercial / industrial buildings 2020	0.782	0.921	0.996	2.360	2.780	3.004
Combustible mass of lightweight buildings 2020	0.587	0.734	0.832	1.770	2.216	2.511
Combustible mass of multi-family buildings 2020	0.417	0.561	0.600	1.259	1.694	1.812
Combustible Mass of inner-city commercial buildings 2020	0.086	0.111	0.111	0.258	0.334	0.334
Combustible mass of highrise buildings 2020	0.021	0.026	0.026	0.064	0.078	0.080
Combustible mass of skyscrapers 2020	0.013	0.015	0.015	0.040	0.046	0.046

https://doi.org/10.5194/essd-2026-401
Preprint. Discussion started: 24 June 2026

Table 3. Combustible mass overview of personal vehicles over time

	Mass (Mt)		**t/capita**		
Year	**combustible**	**non-combustible**	**combustible**	**non-combustible**	**percent combustible**
1975	30.891	182.841	0.149	0.884	14%
1990	53.235	258.267	0.219	1.065	17%
2000	74.319	317.260	0.269	1.148	19%
2020	127.375	368.045	0.384	1.119	26%

4.3 COMBUST-Plus: Population- and building-related exposure variables

COMBUST-Plus contains spatial variables that enable the assessment of building and population exposure to fire-related hazards in combination with the combustible mass estimates of COMBUST. These variables include:

- The built-up surface per grid cell derived from GHSL (Figure 5a)
- Number of buildings per cell derived from Microsoft's USBuildingFootprints data (Figure 5b)
- Number of housing units (derived from ZTRAX; Figure 5c)
- Residential building share (derived from ZTRAX; Figure 5d)
- Share of locally owned properties per grid cell (i.e., where the address of the owner and of the property are identical, derived from ZTRAX; Figure 5e); a particularly useful metric to quantify exposure in cases of weekend of vacation homes where this share is low).
- Measures of the age of the building stock, such as the earliest (Figure 5f) and the average (Figure 5g) construction year per grid cell, derived from ZTRAX.
- Resident population estimates per grid cell (using GHS-POP based on disaggregated U.S. census data; Figure 5h)
- Average cadastral parcel (lot) size per grid cell, as a measure of spacing between buildings (derived from ZTRAX; Figure 5i)
- Estimates of combustible biomass above-ground, below-ground, and total, per grid cell, derived from Spawn et al. (2020); Figure 5,j,k,l.

https://doi.org/10.5194/essd-2026-401
Preprint. Discussion started: 24 June 2026

Open Access Earth System Science Data Discussions

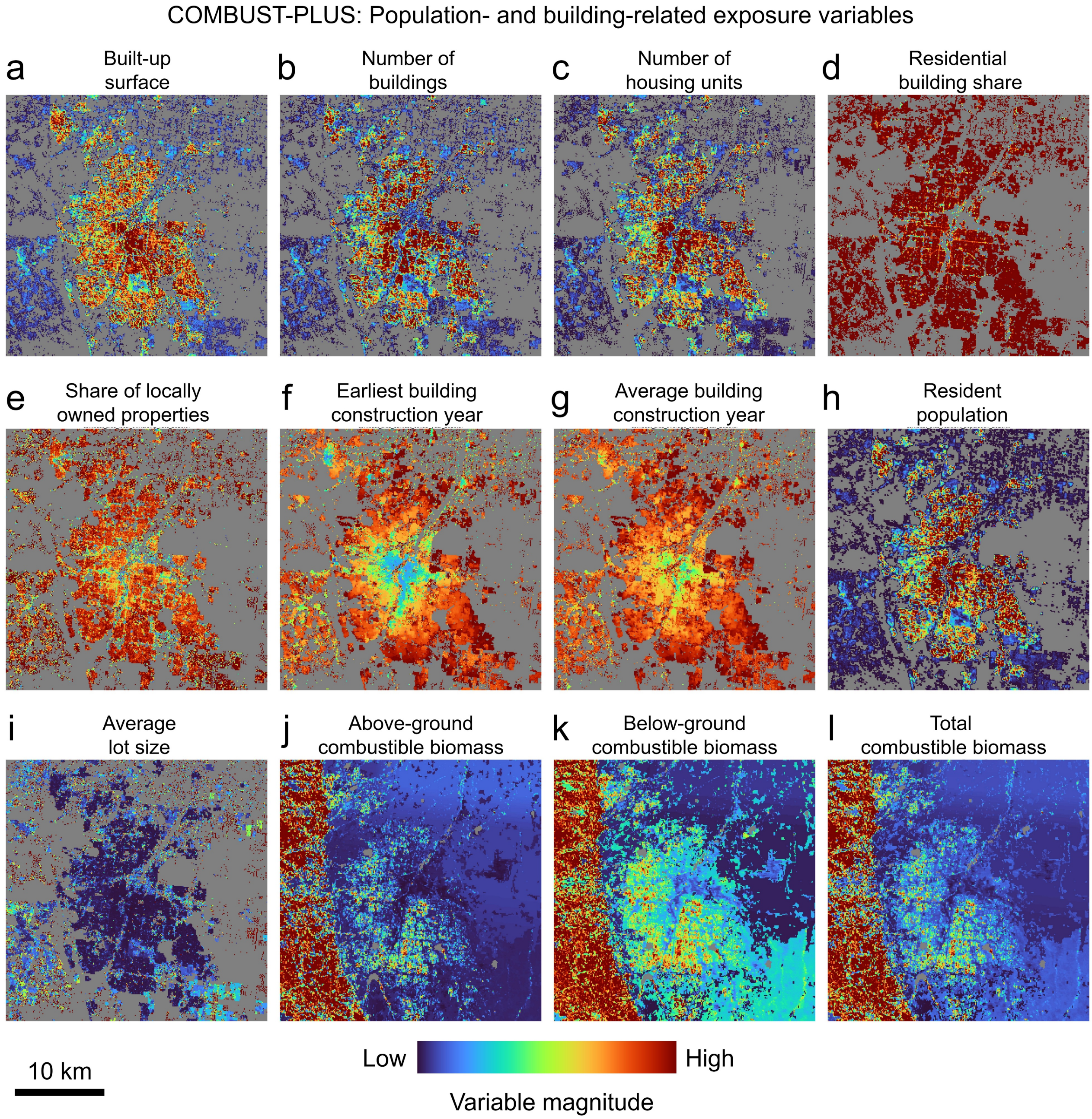

290 **Figure 5. COMBUST-Plus spatial variables of building and population exposure accompanying the COMBUST dataset, obtained from various data sources, integrated and consistently enumerated at 250-m resolution: (a) built-up area, (b) number of buildings, (c) number of housing units, (d) share of residential buildings per cell, (e) share of properties that are locally owned per cell, (f) earliest and (g) average building construction year per grid cell, (h) resident population, (i) average cadastral parcel (lot) size per grid cell, and combustible biomass estimated (j) above-ground, (k) below-ground, and (I) total combustible biomass. Data cover all or large parts of CONUS, and are shown here the Denver metropolitan area.**

https://doi.org/10.5194/essd-2026-401
Preprint. Discussion started: 24 June 2026

Open Access Earth System Science Data Discussions

4.4 Temporal trends of combustible mass

The combustible mass of personal vehicles (0.384 t/capita) in 2020 corresponds to only 1.6% of the total combustible mass. Since 1975, this value has almost tripled (from 0.149 t/capita to 0.384 t/capita), and the percent combustible mass of personal vehicles has increased from 14% in 1975 to 26% in 2020 (Table 3). The combustible mass per capita attributed to gas in gas stations and refineries is even 1 and 2 orders of magnitude lower than that of vehicles, respectively (Table 1).

Looking at the backcasting models, we observe increases of total combustible mass of the building stock roughly ranging between 40% and 50% during the period from 1975 to 2020, from 4 Gt in 1975 to 8 Gt in 2020 (Fig. 6a). Importantly, this increase was approximately linear before 2000, while change rates decreased after 2000. Looking at combustible mass per capita over time (Fig. 6d) across all CONUS, we see an increase in CM/capita from 1975 to approximately 2005, and a slight decrease since then. Our backcasting models assume growth of the built stock over time, disregarding potential shrinkage – hence, the decreasing CM/capita is attributed to growth rates higher for population than for the built stock.

The estimates of total building mass provided by the MSMC data on which the COMBUST estimates are largely based, are provided in three scenarios (low, mean, high), and this spread propagates also into the backcasted CM estimates (Figure 6b,e).

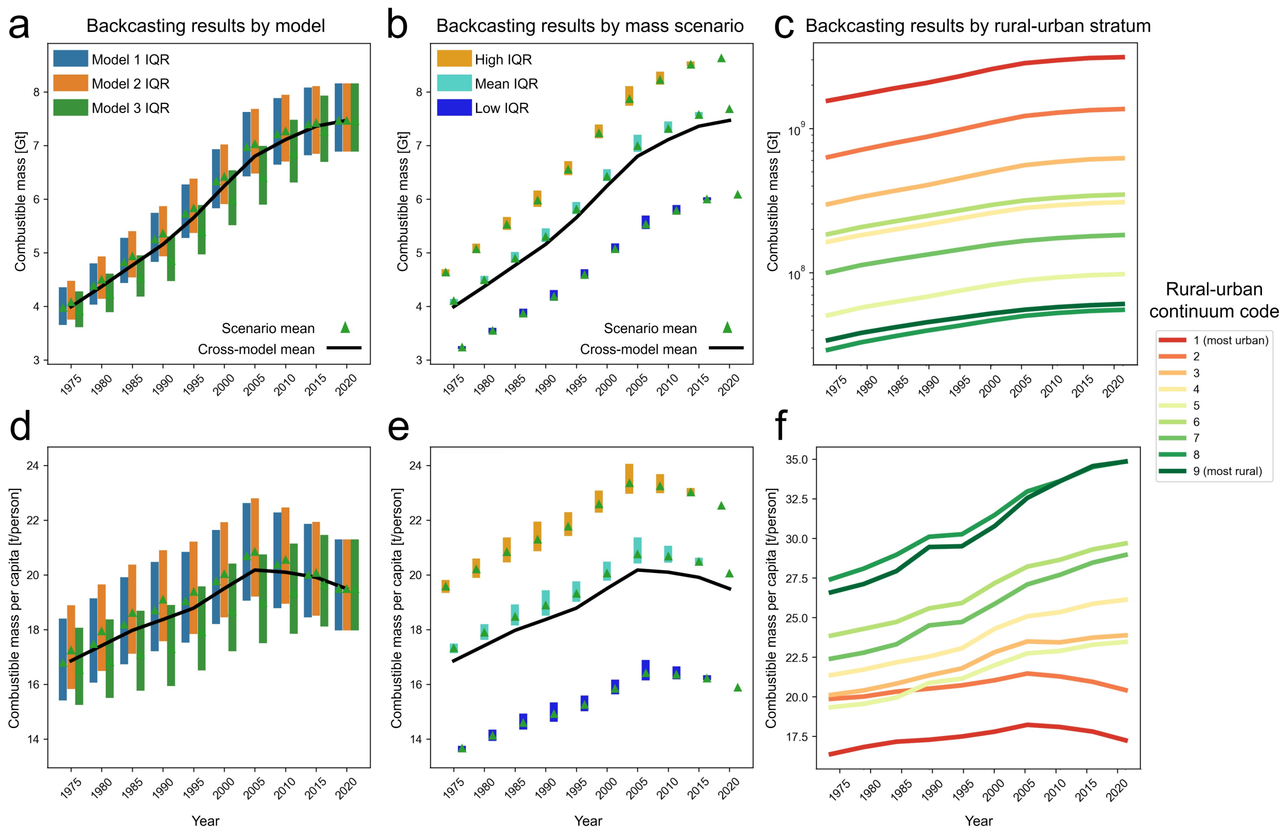

https://doi.org/10.5194/essd-2026-401
Preprint. Discussion started: 24 June 2026

Open Access Earth System Science Data Discussions

Figure 6. Assessment of backcasted combustible mass estimates of building materials, contents, and personal vehicles in CONUS from 1975 to 2020: (a) Boxplots (IQRs only) of total combustible mass per backcasting model aggregated across all building mass scenarios, (b) cross-model IQRs of total combustible mass for each building mass scenario (1975-2020) (c) within rural-urban strata. Panels (d), (e), and (f) show the same data distributions as (a), (b), and (c), however expressed in combustible mass per capita. For rural-urban classification in Panels (c) and (f) we used USDA's county-level urban-rural continuum codes. Backcasting model 1 is based on change rates of building indoor area from HISDAC-US; model 2 is based on change rates of building density from HISDAC-US; and model 3 is based on building volume change rates from GHSL data.

We assume that the decreasing trend of CM/capita since 2005 (Figure 6d,e) is mostly attributed to higher population growth rates. Urbanization and rural outmigration cause urban populations to grow faster, and we assume this trend is dominated by urban strata: We separate the dynamics of CM/capita into metropolitan and non-metropolitan counties (according to the US Census´ core-based statistical area classification), as shown in Table 4. CM/capita in the "mean" scenario has increased by almost 50% from 24 t/capita to 34 t/capita in non-metro counties, while the increase in metro counties from 18.7 t/capita in 1975 to 21.7 t/capita in 2020 corresponds to only 16% - while population in metro counties has increased by 65%, as compared to 27% in non-metro counties (Source: GHS-POP).

Table 4. CM and CM/capita over time and in metro vs non-metro counties.

Year	Scenario	Metropolitan counties		Non-metro counties	
		CM [Gt]	t/capita	CM [Gt]	t/capita
1975	Low	2.559	14.896	0.665	19.012
1975	Mean	3.221	18.746	0.839	23.985
1975	High	3.608	20.999	0.958	27.361
2020	Low	4.906	17.249	1.211	27.220
2020	Mean	6.183	21.738	1.534	34.480
2020	High	6.923	24.340	1.748	39.302

This becomes evident further when looking across the rural-urban continuum, as modelled by USDA´s rural-urban continuum codes (RUCCs, Butler, 1990) (Figure 6c,f): We find that combustible mass has increased across all rural-urban strata, and combustible mass is concentrated in urban strata (Figure 6c). However, CM/capita is higher in rural counties than in urban counties, and CM/capita has largely been steadily increasing in most strata except in the two most urban strata, where we see a decrease in CM/capita after 2000 (Figure 6f), driving the signal observed in the overall trends across CONUS (cf. Figure 6d,e). Steep increases of CM/capita in rural areas are likely a superposed effect of rural population decline alongside rural development by the construction of new buildings.

Finally, we assess the results of the three backcasting models and the total building mass scenarios from Frantz et al. across rural-urban strata (Appendix Figure C1), showing the same trends as observed in Figure 6, but also indicating that the CM/capita estimates in rural strata are affected by higher levels of uncertainty, as the spread between different models and scenarios is higher than in urban strata.

https://doi.org/10.5194/essd-2026-401
Preprint. Discussion started: 24 June 2026

5 Limitations and conclusions

COMBUST represents a unique data source to quantify the combustible mass of the built environment, allowing for measuring building-related emissions in case of wildfires or other fire- or combustion-related hazards. The dataset is based on a multi-source data integration framework, conflating information from various remote-sensing-based and other geospatial datasets covering over 110 million structures in the US.

While the results obtained from COMBUST are highly plausible, some limitations remain: COMBUST inherits uncertainty directly from the source data used from Frantz et al. (2023). Specifically, these data are affected by (a) uncertainty of thematic estimates of building function (e.g., residential, industrial, etc.), (b) uncertainty in the quantitative estimates of building mass and volume, and, potentially, (c) by positional uncertainty due to the quality of georeferencing of underlying remote sensing data. While the latter component has a minor effect due to the aggregation to 250 m grid cells, uncertainty in building function estimates affects the model-based inference of building material composition. According to Frantz et al. (2023), building types are predicted with an overall accuracy of 79.92% (Frantz et al. 2023, Supplementary Table 7). Building mass in Frantz et al. is derived from estimated building volume and material densities. Hence, uncertainty in building volume estimation (defined as building footprint area x building height) affects the quality of mass estimates. Building footprint area estimates were derived from Microsoft´s USBuildingFootprint data (Microsoft, 2021), assumed to be highly accurate (Microsoft, 2021). According to Frantz et al. (2023), their building height estimation based on Sentinel-1 and Sentinel-2 data achieves an average Mean Absolute Error (MAE) of 2.99 m (internal validation) and 3.21 m (external validation). Based on building type and volume, and building-type-specific material compositions and their densities, the total mass is estimated. This overall mass across the United States is estimated as 390 t/capita, which is in line with other studies, that range from 300 t/capita to 430 t/capita (Supplementary Figure 9 of Frantz et al. 2023). While these reported accuracy metrics seem promising, and the plausibility of these mass estimates is high, Frantz et al. (2023) provide upper and lower bounds, and their mean estimate for each grid cell. COMBUST is available for these three scenarios, allowing for evaluating the sensitivity of combustible mass estimates (Figure 6).

Additional uncertainty in COMBUST is introduced by the estimation of combustible mass of building contents using ZTRAX building indoor area and function, following a method proposed by Frishcosy et al. (2021). This method estimates the material composition of building contents based on building function and estimates the total combustible mass using fuel load densities and building indoor area. ZTRAX covers the CONUS built environment well, and areas that are built-up but not covered by construction year information from ZTRAX correspond to approximately 2.7% of the CONUS land mass (Uhl et al., 2021), resulting in approximately 12% of the total combustible mass that cannot be backcasted using the ZTRAX / HISDAC-US based backcasting models. However, this share drops to 0.04% when using the GHSL-based backcasting model. For the grid cells covered by the MSMC data, but not by ZTRAX, we imputed the combustible mass of building contents, introducing additional uncertainty. ZTRAX (or the derived HISDAC-US dataset) agrees well with Microsoft's USBuildingFootprints data along the rural-urban gradient (i.e., an F-score of 0.78 within census places in most rural

https://doi.org/10.5194/essd-2026-401
Preprint. Discussion started: 24 June 2026

counties, and >0.9 in most urban counties, Uhl et al., 2021), indicating a high level of coherence between real-estate data and building footprint data derived from very high-resolution satellite imagery.

For the estimation of historical building counts and building-level emissions from COMBUST, we used building densities derived from HISDAC-US historical building density data (i.e., the BUPL dataset). The accuracy of BUPL time series has been estimated to be above 0.8 (as measured by the F-score) between the years 1975 and 2000 in both rural and urban areas (see Uhl et al., 2021). The backcasting model 3 relies on historical building volume estimates from GHSL. While the vertical component of GHSL building volume estimates is challenging to validate (due to lack of multi-temporal 3D building data), the horizontal component (i.e., built-up surface) measured in GHSL has shown to be highly accurate compared to other global, longitudinal settlement datasets (Pesaresi et al., 2024).

Moreover, the thematic accuracy of COMBUST for discriminating built-up and not built-up grid cells is high, and corresponds to the built-up domain of Microsoft´s USBuildingFootprint dataset (as these data were used as built-up mask in the underlying MSMC data (Frantz et al., 2023). A previous comparison of Microsoft data with authoritative building footprint data for a range of U.S. counties showed an F-score of 0.90 in low-density, and 0.97 in high-density counties (see Appendix F of Uhl et al., 2021). These numbers are also applicable to the coverage of the built-up domain of COMBUST in 2020.

As the estimates of combustible mass of personal vehicles are based on average values using population distribution as a proxy variable, they do not take into account commercially used vehicles such as trucks or buses. In addition to that, the number of vehicle/capita information used to infer the number of cars per grid cell is assumed to be stationary for the whole CONUS, due to lack of more detailed information, while it is likely that the number of vehicles per capita varies across the rural-urban continuum and potentially across income classes.

The total combustible mass per capita in CONUS, as reported in COMBUST, ranges between 15 and 23 t/capita, which is in the same order of magnitude as previous, top-down estimates (i.e., 11t/capita as reported by Toon et al. 2007, 2008). However, our estimates are slightly higher. This could be due to different data availability at the time, the approach used, and the inclusion of building contents in the COMBUST model. Furthermore, our estimates exhibit substantial variations across the rural-urban gradient, which are in line with intra-urban variations found by Frishcosy et al. (2021). Importantly, the backcasted COMBUST data do not take into account buildings that existed in the past but not in 2020 – building stock shrinkage and building stock renewal are not reflected in COMBUST. Future work includes the adaptation and application of the COMBUST method to a global scope, based on available data including spatially-explicit, global material stock estimates (e.g., Haberl et al., 2025).

We anticipate that this dataset will be used to better understand built environment trends in combustible mass, with applications to understanding risk to natural and human-made disasters and social and environmental consequences of resulting injection into the atmosphere, debris flows, and other mechanisms of structure and vehicle degradation. Further application domains include urban planning in the context of sustainable urban development towards resilient urban systems, in the light of increasing risk to hazards in the wildland-urban interface and beyond. COMBUST provides a baseline dataset for modelling structure-based atmospheric emissions due to wildfire events, and for estimating the effects of military interventions including fire spread, exposure and damage estimations resulting from military attacks on infrastructure or civil targets (e.g., Toon et al., 2007). In conclusion, COMBUST provides a valuable and plausible baseline dataset for assessing combustible mass across spatiotemporal trajectories in the conterminous United States, and contributes to a better understanding of the built environment.

Author contributions

OT, JB, SL and JU designed the dataset. JU and MC curated and processed source data, developed model code and performed validation experiments. JU visualized the results. JU, MC, CA, AR, SL, JB and OT wrote the manuscript.

Competing interests

The authors declare no conflict of interest.

Acknowledgments

This work has been supported by the Open Philanthropy Project (OPP) and has benefited from funding through the Human Networks and Data Science –Infrastructure program of the US National Science Foundation (Award Number 2121976) to the University of Colorado Boulder. Moreover, we acknowledge access to the Zillow Transaction and Assessment Dataset (ZTRAX) through a data use agreement between the University of Colorado Boulder and Zillow Group Inc. More information on accessing the data can be found at http://zillow.com/ztrax. The results and opinions are those of the authors and do not reflect the position of Zillow Group. Support by Zillow Group Inc. is acknowledged.

Data and code availability

The COMBUST data are available at https://doi.org/10.5281/zenodo.15611963 (Uhl et al., 2025). Python code for data production is available at https://github.com/johannesuhl/COMBUST.

References

Ahn, Y., Leyk, S., Uhl, J. H., & McShane, C. M.: An integrated multi-source dataset for measuring settlement evolution in the United States from 1810 to 2020. Scientific data, 11(1), 275, 2024.

Barnett, A., Cheng, C., Horasan, M., He, Y., & Park, L.: Fire load density distribution in school buildings and statistical modelling. Fire technology, 58(1), 503-521, 2022.

https://doi.org/10.5194/essd-2026-401
Preprint. Discussion started: 24 June 2026

Baumgart, A., Virág, D., Frantz, D., Schug, F., Wiedenhofer, D.: Material intensity factors for buildings, roads and rail-based infrastructure in the United States. Zenodo, doi:10.5281/zenodo.5045337, 2022.

Burgan, R. E., Klaver, R. W., & Klaver, J. M.: Fuel models and fire potential from satellite and surface observations. International journal of wildland fire, 8(3), 159-170, 1998.

Bush, B., Anno, G., McCoy, R., Gaj, R., & Small, R. D.: Fuel loads in US cities. Fire technology, 27(1), 5-32,1991.

Butler, M. A.: Rural-urban continuum codes for metro and nonmetro counties (No. 9028). US Department of Agriculture, Economic Research Service, Agriculture and Rural Economy Division, 1990.

Che, Y., Li, X., Liu, X., Wang, Y., Liao, W., Zheng, X., ... & Dai, Y.: 3D-GloBFP: The first global three-dimensional building footprint dataset. Earth System Science Data Discussions, 2024, 1-28, 2024.

Chen, B., Wu, S., Jin, Y., Song, Y., Wu, C., Venevsky, S., ... & Gong, P.: Wildfire risk for global wildland–urban interface areas. Nature Sustainability, 7(4), 474-484, 2024.

Coupe, J., Bardeen, C. G., Robock, A., & Toon, O. B.: Nuclear winter responses to nuclear war between the United States and Russia in the whole atmosphere community climate model version 4 and the Goddard Institute for Space Studies ModelE. Journal of Geophysical Research: Atmospheres, 124(15), 8522-8543, 2019.

Davis, S. C., and Boundy, R. G.: Transportation energy data book: Edition 39 (No. ORNL/TM-2020/1770). Oak Ridge National Laboratory (ORNL), Oak Ridge, TN (United States), 2021.

Du, J., Yin, K., Nadim, F., & Lacasse, S.: Quantitative vulnerability estimation for individual landslides. In Proceedings of the 18th international conference on soil mechanics and geotechnical engineering, Paris (pp. 2181-2184), 2013.

Dubayah, R., Blair, J. B., Goetz, S., Fatoyinbo, L., Hansen, M., Healey, S., ... & Silva, C.: The Global Ecosystem Dynamics Investigation: High-resolution laser ranging of the Earth's forests and topography. Science of remote sensing, 1, 100002, 2020.

Dundar, U., & Selamet, S.: Fire load and fire growth characteristics in modern high-rise buildings. Fire safety journal, 135, 103710, 2023.

Esch, T., Brzoska, E., Dech, S., Leutner, B., Palacios-Lopez, D., Metz-Marconcini, A., ... & Zeidler, J.: World Settlement Footprint 3D-A first three-dimensional survey of the global building stock. Remote sensing of environment, 270, 112877, 2022.

Florio, P., Politis, P., Krasnodębska, K., Uhl, J. H., Melchiorri, M., Martinez, A. M., ... & Kemper, T.: GHS-OBAT: Global, open building attribute data reporting age, function, height and compactness at footprint level. Data in Brief, 111751, 2025.

Frantz, D., Schug, F., Wiedenhofer, D., Baumgart, A., Virág, D., Cooper, S., ... & Haberl, H.: Unveiling patterns in human dominated landscapes through mapping the mass of US built structures. Nature Communications, 14(1), 8014, 2023.

Frishcosy, C. C., Wang, Y., & Xi, Y.: A novel approach to estimate fuel energy from urban areas. Energy and Buildings, 231, 110609, 2021.

Gong, P., Li, X., Wang, J., Bai, Y., Chen, B., Hu, T., ... & Zhou, Y.: Annual maps of global artificial impervious area (GAIA) between 1985 and 2018. Remote Sensing of Environment, 236, 111510, 2020.

Haberl, H., Baumgart, A., Zeidler, J., Schug, F., Frantz, D., Palacios-Lopez, D., ... & Esch, T.: Weighing the global built environment: High-resolution mapping and quantification of material stocks in buildings. Journal of Industrial Ecology, 29(1), 159-172, 2025.

Haberl, H., Wiedenhofer, D., Schug, F., Frantz, D., Virág, D., Plutzar, C., ... & Hostert, P.: High-resolution maps of material stocks in buildings and infrastructures in Austria and Germany. Environmental science & technology, 55(5), 3368-3379, 2021.

HIFLD: POL Terminals. Available online https://hub.arcgis.com/datasets/geoplatform::pol-terminals-1/explore. Last access: 01/02/2025, 2025.

Houghton, R. A., Hall, F., & Goetz, S. J.: Importance of biomass in the global carbon cycle. Journal of Geophysical Research: Biogeosciences, 114(G2), 2009.

Leite, R. V., Silva, C. A., Broadbent, E. N., Do Amaral, C. H., Liesenberg, V., De Almeida, D. R. A., ... & Klauberg, C.: Large scale multi-layer fuel load characterization in tropical savanna using GEDI spaceborne lidar data. Remote Sensing of Environment, 268, 112764, 2022.

Leyk, S., & Uhl, J. H.: HISDAC-US, historical settlement data compilation for the conterminous United States over 200 years. Scientific data, 5(1), 1-14, 2018.

Leyk, S., Uhl, J. H., Connor, D. S., Braswell, A. E., Mietkiewicz, N., Balch, J. K., & Gutmann, M.: Two centuries of settlement and urban development in the United States. Science advances, 6(23), eaba2937, 2020.

Ma, X., Zheng, G., Xu, C., Moskal, L. M., Gong, P., Guo, Q., ... & Zhou, Y.: A global product of 150-m urban building height based on spaceborne lidar. Scientific Data, 11(1), 1387, 2024.

Mahmoud, H., & Chulahwat, A.: Unraveling the complexity of wildland urban interface fires. Scientific Reports, 8(1), 9315, 2018.

Marconcini, M., Metz-Marconcini, A., Üreyen, S., Palacios-Lopez, D., Hanke, W., Bachofer, F., ... & Strano, E.: Outlining where humans live, the World Settlement Footprint 2015. Scientific Data, 7(1), 242, 2020.

Marconcini, M., Gorelick, N., Metz-Marconcini, A., & Esch, T.: Accurately monitoring urbanization at global scale–the world settlement footprint. In IOP Conference Series: Earth and Environmental Science (Vol. 509, No. 1, p. 012036). IOP Publishing, 2020.

McWethy, D. B., Schoennagel, T., Higuera, P. E., Krawchuk, M., Harvey, B. J., Metcalf, E. C., ... & Kolden, C.: Rethinking resilience to wildfire. Nature Sustainability, 2(9), 797-804, 2019.

Microsoft: USBuildingFootprints. Available online at https://github.com/microsoft/USBuildingFootprints, 2021.

Mietkiewicz, N., Balch, J. K., Schoennagel, T., Leyk, S., St. Denis, L. A., & Bradley, B. A.: In the line of fire: consequences of human-ignited wildfires to homes in the US (1992–2015). Fire, 3(3), 50, 2020.

National Academies of Sciences, Engineering, and Medicine: Measurement of WUI Fires: Emissions and Exposures. In The Chemistry of Fires at the Wildland-Urban Interface. National Academies Press (US), 2022.

Nolte, C., Boyle, K. J., Chaudhry, A. M., Clapp, C., Guignet, D., Hennighausen, H., ... & Uhl, J. H.: Data practices for studying the impacts of environmental amenities and hazards with nationwide property data. Land Economics, 100(1), 200-221, 2024.

Oostwegel, L. J., Schorlemmer, D., & Guéguen, P.: From Footprints to Functions: A Comprehensive Global and Semantic Building Footprint Dataset. Scientific Data, 12(1), 1699, 2025.

Papini, S., Rao, S. X., & Egger, P. H.: Evolving Cityscape: A Dataset for Building Footprints and Heights from Satellite Imagery in China. Scientific Data, 12(1), 1678, 2025.

Pausata, F. S., Lindvall, J., Ekman, A. M., & Svensson, G.: Climate effects of a hypothetical regional nuclear war: Sensitivity to emission duration and particle composition. Earth's Future, 4(11), 498-511, 2016.

Pesaresi, M., Corbane, C., Ren, C., & Edward, N.: Generalized Vertical Components of built-up areas from global Digital Elevation Models by multi-scale linear regression modelling. PLoS One, 16(2), e0244478, 2021.

Pesaresi, M., Schiavina, M., Politis, P., Freire, S., Krasnodębska, K., Uhl, J. H., ... & Kemper, T.: Advances on the Global Human Settlement Layer by joint assessment of Earth Observation and population survey data. International Journal of Digital Earth, 17(1), 2390454, 2024.

Radeloff, V. C., Helmers, D. P., Kramer, H. A., Mockrin, M. H., Alexandre, P. M., Bar-Massada, A., ... & Stewart, S. I.: Rapid growth of the US wildland-urban interface raises wildfire risk. Proceedings of the National Academy of Sciences, 115(13), 3314-3319, 2018.

Reeves, M. C., Ryan, K. C., Rollins, M. G., & Thompson, T. G.: Spatial fuel data products of the LANDFIRE project. International Journal of Wildland Fire, 18(3), 250-267, 2009.

Robock, A., Oman, L., & Stenchikov, G. L.: Nuclear winter revisited with a modern climate model and current nuclear arsenals: Still catastrophic consequences. Journal of Geophysical Research: Atmospheres, 112(D13), 2007a.

Robock, A., Oman, L., Stenchikov, G. L., Toon, O. B., Bardeen, C., & Turco, R. P.: Climatic consequences of regional nuclear conflicts. Atmospheric Chemistry and Physics, 7(8), 2003-2012, 2007b.

Smith, A. M., Kolden, C. A., Paveglio, T. B., Cochrane, M. A., Bowman, D. M., Moritz, M. A., ... & Abatzoglou, J. T.: The science of firescapes: achieving fire-resilient communities. Bioscience, 66(2), 130-146, 2016.

Spawn, S. A., Sullivan, C. C., Lark, T. J., & Gibbs, H. K.: Harmonized global maps of above and belowground biomass carbon density in the year 2010. Scientific Data, 7(1), 112, 2020.

St. Denis, L. A., Short, K. C., McConnell, K., Cook, M. C., Mietkiewicz, N. P., Buckland, M., & Balch, J. K.: All-hazards dataset mined from the US National Incident Management System 1999–2020. Scientific data, 10(1), 112, 2023.

Stewart, S. I., Radeloff, V. C., Hammer, R. B., & Hawbaker, T. J.: Defining the wildland–urban interface. Journal of Forestry, 105(4), 201-207, 2007.

Stenke, A., Hoyle, C. R., Luo, B., Rozanov, E., Gröbner, J., Maag, L., ... & Peter, T.: Climate and chemistry effects of a regional scale nuclear conflict. Atmospheric Chemistry and Physics, 13(19), 9713-9729, 2013.

https://doi.org/10.5194/essd-2026-401
Preprint. Discussion started: 24 June 2026

Tang, W., Wiedinmyer, C., Emmons, L. K., Holder, A. L., Uhl, J. H., St. Denis, L. A., ... & Levelt, P. F.: Emissions from burned structures in wildfires as significant yet unaccounted sources of US air pollution. Nature Communications 16(11443), 2025.

Toon, O. B., Robock, A., Turco, R. P., Bardeen, C., Oman, L., & Stenchikov, G. L.: Consequences of regional-scale nuclear conflicts. Science, 315(5816), 1224-1225, 2007.

Toon, O. B., Robock, A., & Turco, R. P.: Environmental consequences of nuclear war. Physics Today, 61(12), 37-42, 2008.

Toon, O. B., Bardeen, C. G., Robock, A., Xia, L., Kristensen, H., McKinzie, M., ... & Turco, R. P.: Rapidly expanding nuclear arsenals in Pakistan and India portend regional and global catastrophe. Science Advances, 5(10), eaay5478, 2019.

Turco, R. P., Toon, O. B., Ackerman, T. P., Pollack, J. B., & Sagan, C.: Nuclear winter: Global consequences of multiple nuclear explosions. Science, 222(4630), 1283-1292, 1983.

Turco, R. P., Toon, O. B., Ackerman, T. P., Pollack, J. B., & Sagan, C.: Climate and smoke: An appraisal of nuclear winter. Science, 247(4939), 166-176, 1990.

Uhl, J. H., Leyk, S., McShane, C. M., Braswell, A. E., Connor, D. S., & Balk, D.: Fine-grained, spatio-temporal datasets measuring 200 years of land development in the United States. Earth System Science Data 13-1, 119–153, 2021.

Uhl, J. H., & Leyk, S.: MTBF-33: A multi-temporal building footprint dataset for 33 counties in the United States (1900–2015). Data in Brief, 43, 108369, 2022.

Uhl, J. H., Cook, M., Amaral, C., Leyk, S., Balch, J. K., Robock, A., & Toon, O. B.: COMBUST: Gridded combustible mass estimates of the built environment in the conterminous United States (1975-2020) [Data set]. Zenodo. https://doi.org/10.5281/zenodo.15611963, 2025.

Ural, S., Hussain, E., Kim, K., Fu, C. S., & Shan, J.: Building extraction and rubble mapping for city port-au-prince post-2010 earthquake with GeoEye-1 imagery and lidar data. Photogrammetric Engineering & Remote Sensing, 77(10), 1011-1023, 2011.

Xia, L., Robock, A., Scherrer, K., Harrison, C. S., Bodirsky, B. L., Weindl, I., ... & Heneghan, R.: Global food insecurity and famine from reduced crop, marine fishery and livestock production due to climate disruption from nuclear war soot injection. Nature Food, 3(8), 586-596, 2022.

Zhu, X. X., Li, Q., Shi, Y., Wang, Y., Stewart, A. J., Prexl, J., & Zhang, F.: GlobalBuildingMap—Unveiling the mystery of global buildings. Scientific Data, 13, 71, 2026.

Zillow Inc.: ZTRAX -Zillow Transaction and Assessment Databased. Available online: https://www.zillow.com/research/ztrax/ Last access: 11-11-2025, 2020.

https://doi.org/10.5194/essd-2026-401
Preprint. Discussion started: 24 June 2026

Open Access Earth System Science Data Discussions

Appendices

Appendix A. Modelling combustible mass of building materials

The MSMC data produced by Frantz et al. (2023) is available as 10-m raster data reporting the volume and mass of buildings, per building type. We first resampled (i.e., aggregated) the 10 m volume estimates to the 250 m COMBUST grid. COMBUST is provided at 250 m resolution as many ancillary data, such as HISDAC-US data, are available at that resolution. Based on accompanying information on material intensity factors (in kg / m³; Baumgart et al., 2022), the cell-level total mass per building type was obtained from the total volume and disaggregated into individual material contributions, and re-aggregated into combustible mass per cell and building type, and non-combustible mass per cell and building type (Table A1).

Table A1. Building types used in COMBUST. Source: Baumgart et al., 2022.

Building type (COMBUST)	Category (Baumgart et al. 2022)	Description (from Baumgart et al. 2022)
Single family	RES-LR	(Semi-) Detached residential structure and attached small-scale residential or (rarely) commercial structure with a height lower than 10 m
Multi-family	RES-MR	(Semi-) Detached residential structure and attached small-scale residential or (rarely) commercial structure with a height between 10 and 30 m
Commercial (nner city)	RCMU	Detached and attached medium to large residential, commercial or office structure lower than 30 m
Highrise	RCMU-HR	Detached and attached medium to large residential, commercial or office structure between 30 and 75 m
Skyscraper	RCMU-SKY	Detached and attached medium to large residential, commercial or office structure higher than 75 m (includes skyscrapers)
Commercial / industrial	C/I	Attached or detached light small-scale commercial, industrial or office structure and large industrial or retail and heavy industry
Lightweight	MLB	Mobile homes and detached light-weight buildings such as wooden cabins, huts, garages, etc.

For each building type, Baumgart et al. (2022) provide material intensities for CONUS. For the single family category, these material intensities are reported separately for different climate zones covering the CONUS (Table A.1.2). We used climate zones from the U.S. Department of Energy (https://basc.pnnl.gov/building-assemblies) to apply the climate-zone specific material intensities.

https://doi.org/10.5194/essd-2026-401
Preprint. Discussion started: 24 June 2026

Appendix B. Modelling combustible mass of building contents

Frishcosy et al. (2021) propose a method to estimate the combustible mass of the built environment based on a relatively simple set of input parameters. These parameters include the size (i.e., the areal extent) and the function (i.e., the land use) of a specific unit of land, which could be a census unit or a cadastral parcel of homogeneous land use. For a given land use type, Frishcosy et al. (2021) provide fuel load densities (***FLD***), estimating the energy density of fuel materials in MJ/m². Thus, for a given areal unit $\boldsymbol{a}$ [m²] of known land use $\boldsymbol{lu_a}$, the fuel energy (***FE***) measured in MJ can be estimated as

$$FE_a = a \cdot FLD_{lu} \tag{2}$$

We consider the following land use classes and their associated fuel load densities, as provided by Frishcosy et al., representing median values from various scientific studies (Table B1).

Table B1. Fuel load densities per land use category. Source: Frishcosy et al. (2021).

Land use type	Fuel load density (MJ/m²)
Agriculture	450
Business	500
Commercial	1400
Educational	734
Entertainment	393
Industrial	1018
Residential	848
Utilities	157

Subsequently, based on the fuel energy $\boldsymbol{FE_a}$, we can estimate the mass of the fuels i.e., the combustible mass (***CM***) within the areal unit $\boldsymbol{a}$. To do so, we make two assumptions:

1. Each land use category $\boldsymbol{lu}$ is associated with a specific composition of combustible materials. Thus, for each combustible material $\boldsymbol{m}$, we can estimate its energy contribution $\boldsymbol{EC_m}$, measured in %, as specified in Table B2.
2. For each material $\boldsymbol{m}$, we can estimate its calorific value $\boldsymbol{CV_m}$, i.e., its fuel energy per mass unit, measured in MJ/kg. These calorific values are shown in Table B3.

https://doi.org/10.5194/essd-2026-401
Preprint. Discussion started: 24 June 2026

Table B2. Relative fuel energy contributions (EC) of various materials (m) per land use category. Source: Frishcosy et al. (2021).

Land use	Wood	Paper	Plastic	Cloth
Agriculture	71%	3%	12%	4%
Business	71%	3%	12%	4%
Commercial	42%	8%	32%	8%
Educational	42%	8%	32%	8%
Entertainment	42%	8%	32%	8%
Industrial	24%	11%	51%	10%
Residential	71%	3%	12%	4%
Utility	58%	3%	15%	9%

595 **Table B3. Calorific values associated with specific building materials. Source: Frishcosy et al. (2021).**

Material	Wood	Plastic	Paper	Cloth
CV (MJ/kg)	15.72	35.27	15.63	21.15

Based on the fuel energy $\boldsymbol{FE_a}$, and the calorific values of the materials $\boldsymbol{m}$ contained in the areal unit $\boldsymbol{a}$, we can then estimate the total combustible mass $\boldsymbol{CM_a}$ as

$$CM_a = \sum_{m=1}^{7} EC_m \cdot \frac{FE_a}{CV_m} \tag{3}$$

600 With the total combustible mass being the proportional contributions of fuel energy $\boldsymbol{FE_a}$, divided by the material-specific calorific value $\boldsymbol{CV_m}$ for each of the seven material types $\boldsymbol{m}$. Based on this method, Frishcosy et al. (2021) obtain the combustible mass within census units associated with a given land use type. While this is a valid approach for the estimation of urban fuels and their distribution at the level of an individual city, it has several shortcomings: (a) the approach potentially ignores the heterogeneity of land use within a given areal unit, (b) census units can be extensive in rural areas, as they are based on demographic criteria (e.g., a minimum population size), and (c) the temporal inconsistency of census boundaries impedes the analysis of changes in urban fuels over time.

https://doi.org/10.5194/essd-2026-401
Preprint. Discussion started: 24 June 2026

Open Access Earth System Science Data Discussions

For the above reasons, we implemented a modified version of the method proposed by Frishcosy et al., that aims to account, in part, for these shortcomings.

First, we use the individual property as our analytical unit. As the records in ZTRAX typically represent individually owned real estate objects, such as buildings, or building units (e.g., individually owned apartments within a multi-apartment building), our analytical unit can be associated with a single, homogeneous land use (functional) class. Thus, we estimate the combustible mass at the building / building unit level. Second, we account for the vertical component of the built environment. While the method of Frishcosy et al. (2021)is based on planar areal information, we make use of the indoor area attribute provided in ZTRAX, indicating the total area across all stories of the building. Third, we aggregate the property-level combustible mass into a regular grid, consisting of grid cells of 250 m × 250 m, and thus, use an enumeration unit that is independent of an imposed zoning of land use classes or census units that are defined by different criteria. The use of grid cells as enumeration units allows for multi-temporal urban fuel modelling within spatial entities that are consistent over time, enabling both cross-sectional as well as longitudinal analyses at fine spatial scale. Fourth, we make use of the temporal information provided in ZTRAX, i.e., the construction year of each building. The construction year allows for selecting the buildings that existed in a given year. Thus, we use this temporal attribute to create gridded surfaces measuring the urban fuel at an arbitrary point in time.

Hence, we obtained a tuple for each of the > 130,000,000 property records Z in ZTRAX:

$$Z = \left(X_Z, Y_Z, T_Z, A_Z, LU_Z, CM_Z, FE_Z, CM_{m=1}, \ldots, CM_{m=7} \right) \tag{4}$$

consisting of the geolocation of each property (***X,Y***), its construction year ***T***, the indoor area ***A***, the land use class ***LU***, the total combustible mass ***CM***, the corresponding fuel energy ***FE***, as well as the components of the combustible mass components $\boldsymbol{CM_m}$ of each of the seven material types ***m*** contributing to the property.

We used these tuples as input to create gridded surfaces measuring the combustible mass of the building stock for each year from 1999 to 2020 for most parts of the CONUS, and within temporally consistent grid cells of 250 m spatial resolution. The records were first stratified by their construction year $\boldsymbol{T_Z}$, and the allocation of a property record to its underlying grid cell was done based on the geolocation ($\boldsymbol{X_Z Y_Z}$). We then aggregated (i.e., summed up) the combustible mass $\boldsymbol{CM_Z}$, for all properties within each grid cell and used this value to assign the cell value during the rasterization; this process was carried out for each point in time. Following the same process, we created gridded surfaces of the fuel energy $\boldsymbol{FE_Z}$ and for the fuel energy components for the different building materials under consideration.

https://doi.org/10.5194/essd-2026-401
Preprint. Discussion started: 24 June 2026

Appendix C. Backcasting results over time and across the rural-urban continuum

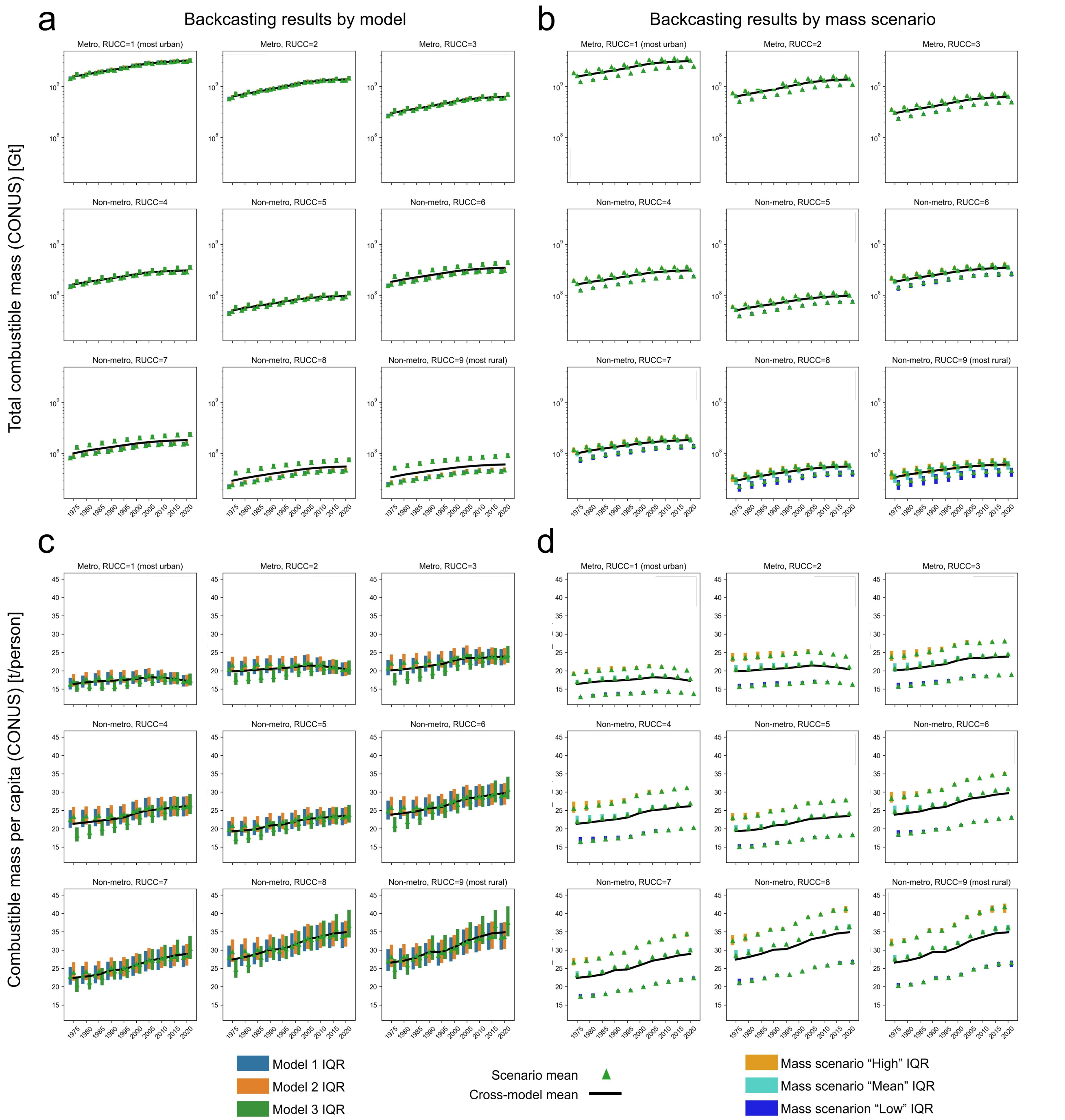

Figure C1. Spread of combustible mass across rural-urban continuum codes, expressed in total combustible mass of CONUS (a) per backcasting model, and (b) per building mass scenario; Panels (c) and (d) show these trends for combustible mass per capita. Backcasting model 1 is based on change rates of building indoor area from HISDAC-US; model 2 is based on change rates of building density from HISDAC-US; and model 3 is based on building volume change rates from GHSL data.